APPLIED ORGANOMETALLIC CHEMISTRY
*Appl. Organometal. Chem.* **14**, 453–464 (2000)

# Perhydridosilicone films produced by IR laser-induced chemical vapour deposition from disiloxane

Josef Pola,[1]* Zdeněk Bastl,[2] Markéta Urbanová,[2] Jan Šubrt[3] and Helmut Beckers[4]

[1]Institute of Chemical Process Fundamentals, Academy of Sciences of the Czech Republic, 165 02 Prague 6, Czech Republic
[2]J. Heyrovský Institute of Physical Chemistry, Academy of Sciences of the Czech Republic, 182 23 Prague 8, Czech Republic
[3]Institute of Inorganic Chemistry, Academy of Sciences of the Czech Republic, 25 068 Řež, near Prague, Czech Republic
[4]Anorganische Chemie, FB 9, Universität-GH, D-5600 Wuppertal 1, Germany

**Solid perhydridosilicone films have been produced by transversely excited atmospheric (TEA) and continuous-wave $CO_2$ laser-induced gas-phase decompositions of $H_3SiOSiH_3$ controlled by elimination and polymerization of transient silanone $H_2Si{=}O$ and affording silane and hydrogen as side products. The decomposition mechanism is supported by evidence of scavenged intermediates and minor volatile products. The films are characterized by FT infrared and x-ray photoelectron spectroscopy and by scanning electron microscopy and shown to undergo facile oxidation of the topmost layers in air and chemical changes upon argon ion sputtering. Copyright © 2000 John Wiley & Sons, Ltd.**

**Keywords: chemical vapour deposition; disiloxane, thin films; laser irradiation**

*Received 25 March 2000; accepted 8 May 2000*

## INTRODUCTION

Polymeric $(H_2SiO)_n$ and $(HSiO_{1.5})_n$ perhydridosiloxanes were prepared by hydrolysis of halogenosilanes many decades ago[1–3] and produced by reaction of disiloxane with ammonia[4] and in gas-phase UV lamp- or IR laser-induced photolyses of silane in the presence of NO.[5,6] They found little use and were paid much less attention than their peralkylated counterparts. Structurally similar materials (thin films of hydrogenated silicon suboxides $SiO_x$:H) are, however, important materials in applied research. Up to now, they were prepared only by plasma-assisted chemical vapour deposition from inert gas-diluted mixtures of silane and oxygen (e.g. Refs 7, 8) or by oxidation of hydrogenated silicon films.[9]

We have recently reported on the use of gaseous disiloxane, $H_3SiOSiH_3$, as a precursor to structurally different hydrogenated silicon suboxide films: a-$Si_2O$:H films with structure close to -$(H_2Si\text{-}O\text{-}SiH_2)_n$-[10] were obtained from disiloxane photolysed by ArF laser radiation; and poly(perhydridosiloxane)—$(H_2SiO)_n$—films[11] were gas-phase deposited from disiloxane decomposed by radiation from a continuous-wave (cw) $CO_2$ laser. While the former process is more difficult due to low absorption of disiloxane at 193 nm, the IR laser decomposition is a feasible reaction whose course can be affected by parameters of the $CO_2$ laser radiation.

In this paper we present our results on the IR laser decomposition of disiloxane (DSO) by pulsed and cw irradiation from $CO_2$ lasers, and reveal the dependence of the properties of the poly(hydridosiloxane) obtained films on the parameters of this laser radiation.

## EXPERIMENTAL

The experiments were performed using a transver-

* Correspondence to: Josef Pola, Laser Chemistry Group, Institute of Chemical Process Fundamentals, Academy of Sciences of the Czech Republic, 165 02 Prague 6, Czech Republic.
E-mail: pola@icpt.cas.cz
Contract/grant sponsor: Grant Agency of the Academy of Sciences of the Czech Republic; Contract/grant number: A4072806.
Contract/grant sponsor: Deutsche forschungsgemeinschaft.
Contract/grant sponsor: Fonds der chemischen Industrie.

sely excited atmospheric (TEA) $CO_2$ laser (Plovdiv University) and a cw $CO_2$ laser (Synrad, model E48-1-28 W), the first operating at the P(12) or P(18) line of the 00 °1→10 °0 transition (951.2 or 946.0 $cm^{-1}$, respectively) with repetition frequency of 1 Hz, and the second operating in the range 934–952 $cm^{-1}$. The wavelengths of the IR radiation were checked with a model 16-A spectrum analyser (Optical Engineering Co., Santa Rosa, CA). The pulse energy and energy output of the laser radiation were determined using a pyroelectric detector (model ml-1 JU, Charles University) and laser power probe (Optical Engineering Co., model 25 A), respectively.

The TEA $CO_2$ laser irradiation of DSO (0.7 kPa) with a fluence of 0.1–0.5 J $cm^{-2}$ was conducted in a Pyrex reactor (length 10 cm, i.d. 2.5 cm) equipped with KBr windows and a valve enabling it to be filled with DSO and other components ($SF_6$, He, Ar), and also making it possible to withdraw samples after irradiation for GC and GC–MS analysis. This irradiation was carried out in the absence or excess helium or argon (each 12 or 100 kPa).

The cw $CO_2$ laser irradiation of DSO (3 kPa) with an incident energy of 80 W $cm^{-2}$ was performed in a Pyrex reactor consisting of two orthogonally positioned tubes (both 2 cm in diameter, one 4 cm long fitted with quartz plates and the other 3 cm long fitted with KBr windows). This reactor was furnished with a port for a pressure transducer and equipped with two PTFE valves. A beam from the cw $CO_2$ laser entered through the KBr window, and UV absorption in the irradiated zone of the gaseous content of this reactor was measured when the laser was on and off by using a miniature fibre-optic UV/Vis spectrometer (Ocean Optics, model ST 1000). For this purpose, fiber collimating lenses were adjusted to control the region closely behind the KBr entrance window. The spectrometer was operated in episodic mode with a scanning period of 80 ms.

The progress of the decomposition of DSO was monitored by periodically removing the reactors from the laser beam and placing them in the Fourier transform infrared (FTIR) spectrometer (Nicolet Impact 400). The pressure of the decomposed DSO and of the silane formed was determined using absorption bands at 2169 and 908 $cm^{-1}$, respectively. The absorption coefficients of both compounds were ascertained by measuring the spectra of pure samples. The gaseous samples obtained by DSO irradiation were also analysed on a Shimadzu 14A chromatograph coupled with a Chromatopac C-R5A data processor, using flame ionization detection (FID), Porapak or SE-30 columns, helium or nitrogen as carrier gas, and programmed (20–150 °C) temperature. Hydrogen was identified on a Hewlett-Packard 5010A gas chromatograph with thermal conductivity detection (TCD), and a Carbosieve column.

Trapping experiments for identifying intermediate $H_2SiO$ species were carried out by TEA $CO_2$ laser irradiation of DSO (0.9 kPa) in an excess of dimethyl(dimethoxy)silane (10 kPa), hexamethyldisiloxane (7 kPa), 1-methyl-1-silacyclobutane (8 kPa), 1,1-dideuterio-1-silacyclobutane (SCB-$d_2$, 8 kPa) or trimethylchlorosilane (7.5 kPa). Volatile products were analysed by GC–MS spectroscopy.

To evaluate the properties of the deposit by FTIR and X-ray photoelectron spectroscopy (XPS), X-ray excited Auger electron spectroscopy (XAES) as well as scanning electron microscopy, the solid materials were deposited from the gas phase on various substrates (Cu, KBr) accommodated in the reactors before the irradiation.

The photoelectron spectra were recorded in a VG ESCA 3 Mk II electron spectrometer. The XPS measurements were performed using an Al $K_\alpha$ ($h\nu$ = 1486.6 eV non-monochromatized source at a power of 220 W. X-ray excited Auger electron spectra were measured using *Bremsstrahlung* radiation. The spherical sector analyser was operated in the fixed analyser transmission mode using a pass energy of 20 eV. The background pressure during the spectrum accumulation was accomplished using a Gaussian–Lorentzian line shape and a damped non-linear least-squares procedure.[12] The concentrations of the elements were quantified by correcting the photoelectron peak areas for their cross-sections[13] and accounting for the dependence of analyser transmission[14] and electron inelastic mean free paths[15] on the kinetic energy of the photoelectrons. The accuracy of the measured binding energies was ±0.2 eV.

Scanning electron microscopy studies of the deposits were performed on an ultrahigh-vacuum instrument (Tesla BS 350).

DSO was prepared by reaction of iodosilane with silver oxide in a vacuum manifold. It was separated from iodosilane by low-temperature distillation. DSO-$d_6$ was obtained by a similar procedure using iodosilane-$d_3$ as starting material. Purity of both compounds (better than 98%) was checked by gas chromatography and a GC–MS technique, and isotopic purity of DSO-$d_6$ was checked by FTIR spectroscopy.

Sulfur hexafluoride (Fluka), silane (Lachema),

 

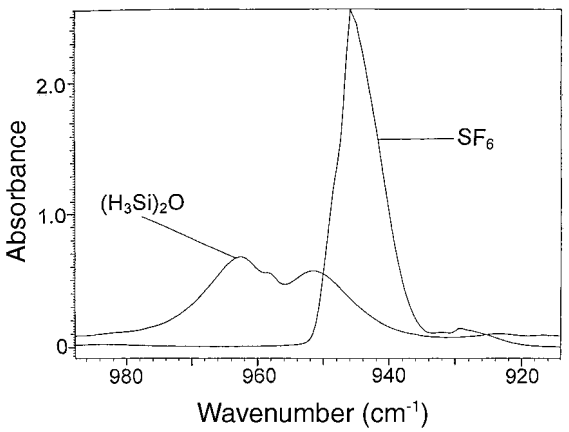


**Figure 1** FTIR spectrum of DSO and $SF_6$ in the emission region of the $CO_2$ laser. Pathlength 10 cm, each constituent at 0.13 kPa.

helium, argon and nitrogen (all Linde) were purchased. Chemicals used as the trapping reagents (Prague) as well as the silane isotopomers $H_nSiD_{4-n}$ ($n = 0$–4) (Wuppertal) were from the laboratory stocks.

## RESULTS AND DISCUSSION

DSO can be decomposed by the radiation of the TEA and cw $CO_2$ lasers due to efficient absorption of the laser radiation in a strong $\delta(H_3Si)$ absorption band.[16,17] The DSO decomposition by the TEA $CO_2$ laser in the presence of $SF_6$ apparently takes place through primary absorption in $SF_6$ as a photosensitized process,[18] since the absorptivity of $SF_6$ at 934–952 $cm^{-1}$ is significantly higher than that of DSO (Fig. 1). The TEA $CO_2$ laser or cw-$CO_2$ laser irradiation at the IR transition of the $\delta(H_3Si)$ mode of DSO (0.7–5.5 kPa) in the absence or presence of helium or argon lead to the formation of gaseous silane ($SiH_4$) and a solid material manifesting itself as thin transparent films or thicker whitish layers deposited from the gas phase on the inside of the reactors.

### TEA $CO_2$ laser-induced decomposition of DSO

Typical IR spectral changes taking place upon TEA $CO_2$ laser irradiation of DSO (Runs 1–6 in Table 1) are given in Fig. 2. With the pulsed radiation, a visible luminescence was observed after each pulse within the narrow area restricted by the laser beam. A residual pressure in the irradiated cell after freezing the volatile compounds (silane and DSO) in a trap cooled with liquid nitrogen indicated the presence of hydrogen that was proved by gas chromatography.

The amount of silane produced depends on the pulsed radiation conditions, but it practically does not alter with the decomposition progress. While the highest yield (*ca* 90 mol%) of silane is obtained with unfocused pulses passing into DSO in an excess of helium, *ca* 60 mol% silane yield is

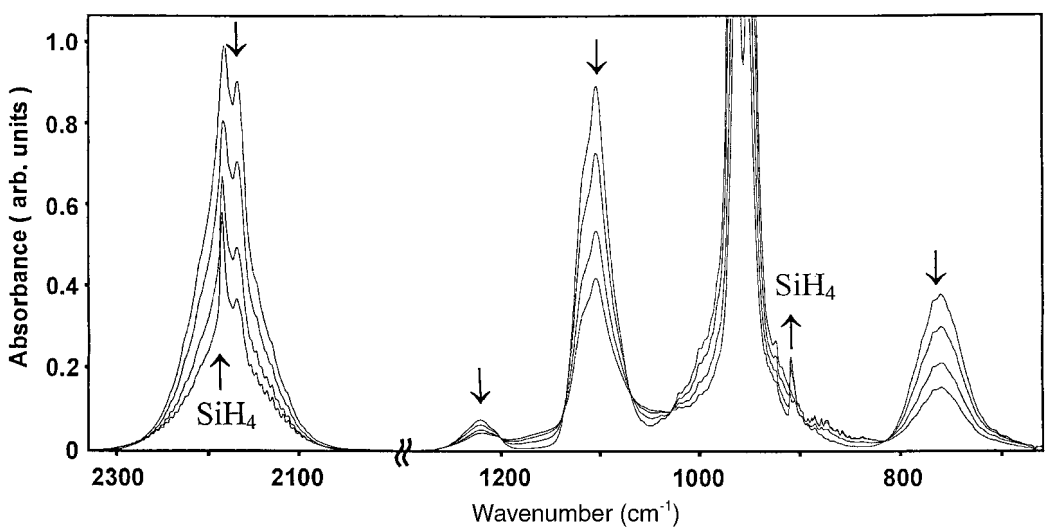


**Figure 2** FTIR spectral changes upon TEA $CO_2$ laser irradiation of DSO (run 5, Table 1; number of pulses: 0, 10, 50 and 100).

 

**Table 1** FTIR spectra of the deposits obtained under various irradiation conditions

| | | Absorptivity[a] | | | | | |
|---|---|---|---|---|---|---|---|
| | | $\delta$(Si–H) | | | $\nu$ (Si–O–Si) | $\nu$ (Si–H) | |
| Run | Irradiation conditions[a] | 803 $cm^{-1}$ | 870 $\pm$ 2 $cm^{-1}$ | 980 $\pm$ 2 $cm^{-1}$ | 1086 $\pm$ 4 $cm^{-1}$ | 2183 $\pm$ 2 $cm^{-1}$ | 2250 $\pm$ 4 $cm^{-1}$ |
| 1 | TEA $CO_2$ laser, Incident fluence 0.1–0.2 J $cm^{-2}$ DSO (0.7 kPa) | 0.18 | 0.25 | 0.20 | 1 | 0.26 | 0.09 |
| 2 | TEA $CO_2$ laser Incident fluence 1.0 J $cm^{-2}$ DSO (0.7 kPa) | 0.17 | 0.31 | 0.07 | 1 | 0.11 | 0.10 |
| 3 | TEA $CO_2$ laser Incident fluence 1.1 J $cm^{-2}$ DSO (4 kPa) | 0.23 | 0.26 | 0.06 | 1 | 0.09 | 0.07 |
| 4 | TEA $CO_2$ laser Incident fluence 1.0 J $cm^{-2}$ DSO (0.7 kPa), Ar (12 kPa) | 0.15 | 0.23 | 0.08 | 1 | 0.11 | 0.07 |
| 5 | TEA $CO_2$ laser Incident fluence 1.0 J $cm^{-2}$ DSO (0.7 kPa), He (12 kPa) | 0.15 | 0.25 | 0.09 | 1 | 0.12 | 0.08 |
| 6 | TEA $CO_2$ laser Incident fluence 1.1 J $cm^{-2}$ DSO + $SF_6$ (both 2 kPa) | 0.02 | 0.32 | 0.15 | 1 | 0.08 | 0.06 |
| 7 | Cw $CO_2$ laser Incident output 80 W $cm^{-2}$ DSO (5.5 kPa) | — | 0.44[b] | 0.13 | 1 | 0.22 | 0.15 |
| 8 | Cw $CO_2$ laser Incident output 50 W $cm^{-2}$ DSO (5.5 kPa) | — | 0.45[b] | 0.12 | 1 | 0.27 | 0.18 |

[a] Normalized to that of the $\nu$ (Si–O) band.
[b] At 864 $\pm$ 2 $cm^{-1}$.

observed with unfocused pulses passing into DSO, *ca* 40 mol% of silane is seen with focused pulses passing into DSO in an excess of argon, or focused pulses passing into DSO without inert gas, and only *ca* 25 mol% yield is observed with the pulses passing into the mixture of DSO and $SF_6$ (Fig. 3). These differences can be explained by there being different effective temperatures for the DSO decomposition. Non-isothermal conditions of the IR laser-powered decompositions were controlled,[19] apart from convection currents, by the thermal conductivity of the gas in excess; we infer that, similarly to the laser decomposition of 2-nitromethane,[20] the highest peak temperatures are achieved with focused pulses, in the presence of $SF_6$ and in an excess of argon, whilst the lowest temperatures are attained in an excess of helium. The fact that the yield of silane is lower than 100% can be rationalized in terms of silane decomposition[21–24] to $H_2$ and a solid Si/H and $Si^0$ material, which is favoured at higher temperatures. The identification of a $Si^0$ form in the deposit (see

 

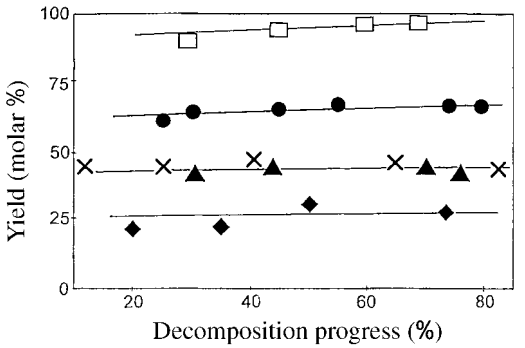


**Figure 3** Dependence of molar yield of silane on progress of TEA $CO_2$ laser-induced decomposition of DSO: □, run 5; ●, run 1; ×, run 4; ▲, run 2; ◆, run 6 conditions as in Table 1.

below) confirms this view. The volatile products observed as well as the solid deposits (see below) suggest that (i) the irradiated DSO decomposes into silane and a short-lived silanone $H_2Si{=}O$ which undergoes polymerization and that (ii) secondary reactions in the irradiated system are dehydrogenation of silane and/or $H_2SiO$ species.

## cw $CO_2$ laser-induced decomposition of DSO

The absorption in DSO of the cw $CO_2$ laser radiation (Runs 7, 8 in Table 1) also affords silane, hydrogen and a solid material deposited on the inside of the reactor. This decomposition has been described in our previous paper.[11] The yields of silane (in mol%) within the 80% decomposition progress is 0.75–0.90. As in the TEA $CO_2$ laser-induced DSO decomposition, this value is lower than 1 and indicates a minor silane decomposition into $H_2$ and a solid Si/H and $Si^0$ material.

## Properties of solid deposits

The deposited films from the cw and TEA $CO_2$ laser irradiation of DSO show IR absorptions (Fig. 4) which are typical for poly(hydridosiloxanes) $H_xSi_yO_z$ and which can be interpreted[7,9,25] in terms of contributions from vibrational modes as compiled in Table 1. They are dominated by a very strong and broad band due to the $\nu$(Si–O–Si) mode at *ca* 1086 $cm^{-1}$ and several minor bands assignable to vibrations of the $H_nSi(O)$ moiety at 803, 870, 980, 2183 and 2250 $cm^{-1}$. In discussing these spectral features we note that the oxygen and $H_nSi$ bending modes below 1000 $cm^{-1}$, reported earlier in amorphous $SiO_x$:H films ($x < 2$) and oxygenated

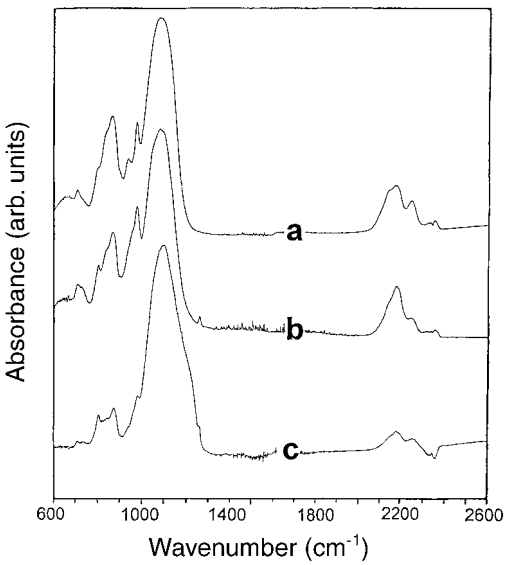


**Figure 4** FTIR spectra of deposit obtained by irradiation of DSO with a cw $CO_2$ laser (run 7; **a**) and a TEA $CO_2$ laser (runs 1 and 3; **b** and **c**, respectively). Conditions as in Table 1.

polysilanes,[26–29] are less informative,[30] while the Si–H stretching mode in polysilanes is empirically related to the electronegativity/inductive effect of the neighbouring atoms,[7,25] and that fully oxidized $(SiH_2)_x$ polysilanes exhibit[9] bands at 2190 and 2245 $cm^{-1}$. The bands at 2183 and 2250 $cm^{-1}$ observed in the films deposited from DSO can thus be unambiguously assigned to the $H_2Si(O)$ structural unit. The lack of bands at *ca* 2100 and 2000 $cm^{-1}$ associated with the absence (or an insignificant content) of $(SiH_2)_n$ and $(SiH)_n$ structures[9,31] in which the Si–H bond is isolated from oxygen by at least two silicon atoms should be noted.

The difference in absorptivity of the $\nu$(Si–H) absorption bands as compared with that of the $\nu$(Si–O–Si) band in the deposits obtained under different irradiation conditions (Table 1) reflects the different content of hydrogen: relatively high hydrogen concentrations relate to the cw laser (Runs 7, 8) and unfocused (low incident fluence) pulsed laser (Run 1) irradiation, while low H-concentrations are seen for the focused (high incident fluence) irradiations (Runs 2–5) or the irradiation in the presence of $SF_6$ (Run 6). In an attempt to estimate the relative content of the Si–O and Si–H bonds we compare the $A_{Si-H}/A_{Si-O-Si}$ ratio in the deposits (0.09–0.26; Table 1) with that in cyclotetrasiloxane $(H_2SiO)_4$ (*ca* 0.5; Ref. 32). This comparison indicates that the

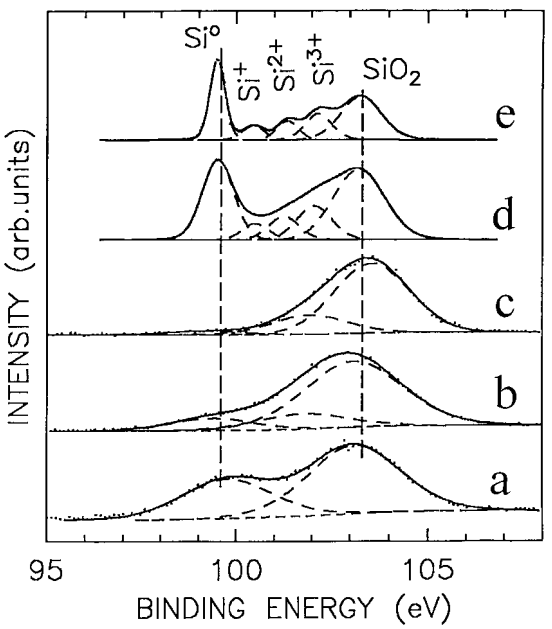


**Figure 5** Fitted photoelectron spectra of Si(2*p*) electrons. (**a**) Authentic sample of SiO (Fluka); (**b**) run 5; (**c**) run 4; (**d**) spectrum obtained from spectrum (**e**) by its convolution with the Gaussian function of 1.2 eV fwhm to obtain the spectrum corresponding to the instrumental resolution of the spectrometer used in this work; (**e**) high-resolution spectrum of the $SiO_2$/Si interface obtained with monochromatized radiation.

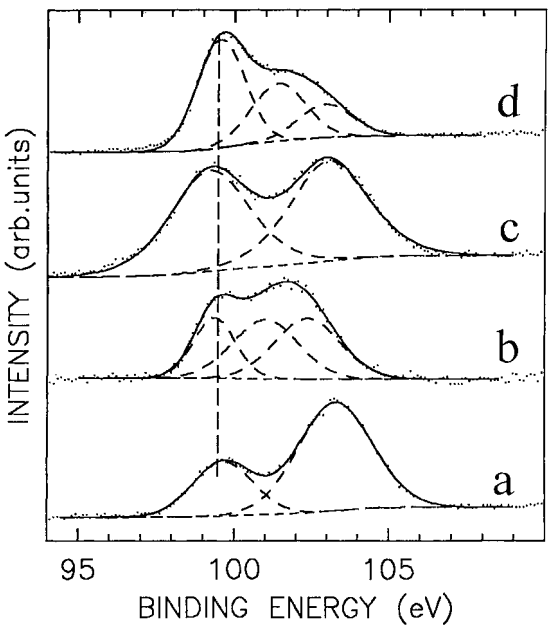


**Figure 6** Fitted photoelectron spectra of Si(2*p*) electrons. (**a**) Run 1; (**b**) the same sample sputtered by argon ions ($E = 4.5$ keV, $I = 35\ \mu$A, $t = 3$ min); (**c**) run 3; (**d**) the same sample sputtered by argon ions ($E = 4.5$ keV, $I = 35\ \mu$A, $t = 3$ min).

deposited films cannot be represented exactly by the $(H_2SiO)_n$ formulae, but rather correspond to a moderately crosslinked polymeric material possessing less hydrogen. The cross-linked structure of the polymeric films is supported by their insolubility in toluene, acetone and methanol.

The photoelectron spectra of the Si(2*p*) electrons (Figs 5, 6), as well as the spectra of the $KL_{23}L_{23}$ Auger electrons (Figs 7, 8) of the deposits produced by the pulsed laser radiation and their comparison with the spectra of the well-defined standard, point to the presence of the three chemical states of Si: $Si^0$, $Si^{4+}$ and $Si^{x+}$ $(0 < x < 4)$. Due to the quasi-amorphous structure of the deposits, the electron spectra are rather broad and consequently the peak belonging to suboxides $Si^{x+}$ cannot be deconvoluted into the contributions of the individual components corresponding to well-defined oxidation states of Si. The population of the assigned chemical states of Si calculated from the peak intensities as well as the overall stoichiometry characterized by O/Si atomic ratios for the measured deposits, along with the data for refer-

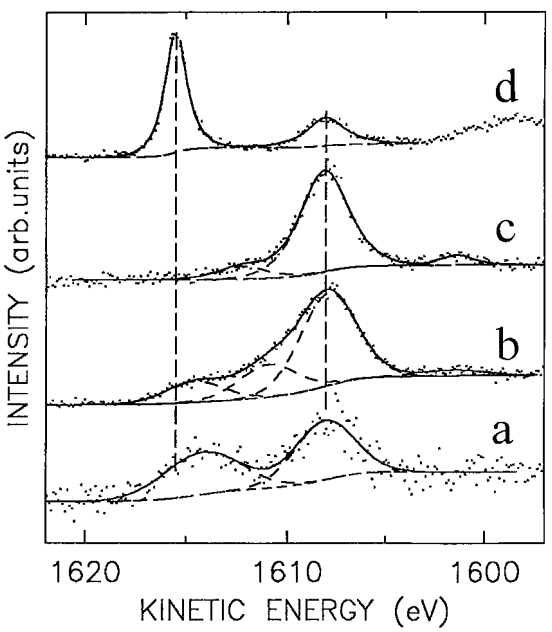


**Figure 7** Fitted spectra of Si ($KL_{23}L_{23}$) Auger electrons. (**a**) Authentic sample of SiO; (**b**) run 5; (**c**) run 4; (**d**) n-Si(111) with native oxide layer.

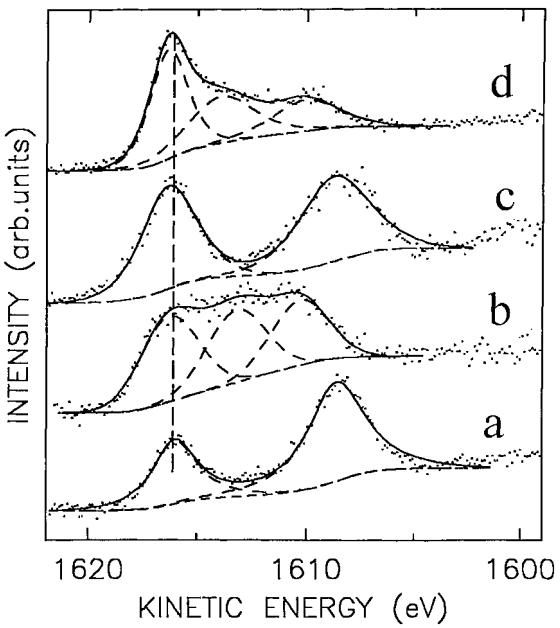


**Figure 8** Fitted spectra of Si ($KL_{23}L_{23}$) Auger electrons. (**a–d**) Conditions as in Fig. 6.

ence samples, are summarized in Table 2. The O/Si ratio in all the deposits is close to 1 or somewhat higher. The layers beneath the topmost ones exposed by argon ion sputtering have an O/Si ratio of 1, which is in accord with the polymerization of $H_2SiO$ or $H_nSiO$ ($n < 2$) species. The higher O/Si values observed with deposits not treated with argon ions indicate incorporation of oxygen in superficial (*ca* 5 nm thick) layers, which is also the case for the SiO sample. The surface oxidation is corroborated by the presence of the higher proportion of the $Si^{4+}$ form in the native films and by its decrease upon argon ion sputtering. The presence of the $Si^0$ form is in line with the observed partial decomposition of silane, and also with the earlier reported $CO_2$ laser-induced decomposition of silane to a:SiH or $Si^0$ solids (e.g. Refs 21, 22, 33, 34). We admit that the formation of $Si^0$ may take place partly from $H_2SiO$ or $H_nSiO$ species, since this $Si^0$ form has also been produced upon interaction of intense $CO_2$ laser fields with alkoxysilanes incorporating similarly strong Si–O bonds.[35] The fraction of $Si^0$ depends on the irradiation conditions: it is higher in the deposits produced by the pulsed radiation in the absence of inert gas and very low in the deposits formed upon pulsed irradiation in argon (Run 4) or cw irradiation (Run 8).

In Table 2, the values of the modified Auger parameter $\alpha'$, defined as the sum of the kinetic energy of the Auger ($KL_{23}L_{23}$) electrons and the binding energy of the Si(2*p*) electrons, are also displayed. According to the literature[36,37] the advantage of the use of Auger parameters, besides its independence of the static surface charging and the choice of the reference level, is that it makes it possible to determine the stoichiometry of Si suboxides more accurately than by calculation from intensities of O (1*s*) and Si (2*p*) photoemission peaks (the results obtained by the latter method may

**Table 2** The surface O/Si atomic ratio, modified Auger parameter $\alpha'$ and population (*p*) of Si oxidation states in deposits and in the standards measured as received

| | | $\alpha'$ (eV) | | | *P* (at.%) | | |
|---|---|---|---|---|---|---|---|
| Run | O/Si | $Si^0$ | $Si^x$ | $Si^{4+}$ | $Si^0$ | $Si^x$ | $Si^{4+}$ |
| 1 | 1.3 | 1715.4 | — | 1711.5 | 28 | — | 72 |
| 1 (Ar)[a] | 1.0 | 1715.9 | 1714.8 | 1712.8 | 22 | 39 | 39 |
| 3 | 1.0 | 1715.4 | — | 1711.6 | 43 | — | 57 |
| 3 (Ar)[a] | 0.6 | 1715.9 | 1715.3 | 1713.0 | 45 | 33 | 22 |
| 4 | 1.4 | — | 1712.5 | 1710.3 | — | 20 | 80 |
| 5 | 1.4 | 1714.1 | 1712.9 | 1711.0 | 14 | 22 | 64 |
| 7 | 1.0 | 1714.8 | 1713.5 | 1711.6 | 20 | 16 | 64 |
| 8 | 1.3 | 1715.2 | 1713.4 | 1711.8 | 5 | 18 | 77 |
| $SiO_2/Si$[b] | — | 1715.4 | | 1711.9 | | | |
| SiO[c] | 1.4 | | 1713.8 | 1711.8 | | 36 | 64 |
| $SiO_2$[c] | 2.0 | | | 1710.7 | | | 100 |

[a] Sample sputtered by Ar ions ($E$ = 4.5 keV, $I$ = 35 $\mu$A, $t$ = 3 min).
[b] Sample of n-Si(111) with a layer of native oxide.
[c] Authentic samples (manufactured by Fluka).

 

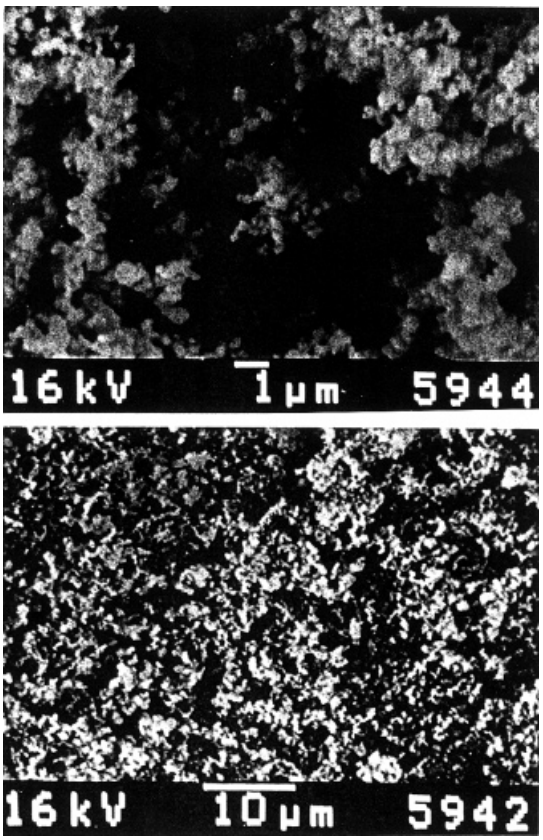


**Figure 9** SEM of the deposit obtained in run 8.

be influenced by the presence of gases adsorbed on the sample surface). The surface contaminations can be removed by ion sputtering[38] which can not only remove the surface layers of the sample but can also cause alteration of the surface composition of some oxides and changes in the chemical states of the elements present.[39] For $SiO_2$, we observed only broadening of the spectral lines after ion sputtering with no change in the surface stoichiometry. In contrast to this result, significant changes of the electron spectra (Figs 6, 8) and surface composition are observed for laser deposits, even after quite short sputtering times. Appearance of the additional chemical state of Si is seen in the spectra. At the same time the Si(2*p*) peak attributed to $Si^{4+}$ shifts towards lower binding energy. The modified Auger parameter for the state created by sputtering is $0.8 \pm 0.3$ eV lower that that obtained for $Si^0$. Using the suggested[36,37] linear correlation between the Auger parameter and oxide composition we arrive at the composition $SiO_{0.3 \pm 0.1}$ for this state while the corresponding binding energy of the Si(2*p*) electrons, 101.2 eV, can be assigned to $Si^{2+}$. We note that similar behaviour, i.e. the appearance of a new chemical state of Si induced by ion sputtering, is also observed (Bastl Z, Drínek V, Senzlober H, Bürger H, Pola J. Unpublished results) for the authentic sample of SiO. These results indicate that (i) the value of the Auger parameter is not only determined by the oxidation number of Si but depends also on the details of oxygen bonding and (ii) the deposited layers possessing an Si–O arrangement with H- atom neighbours show remarkable aptitude to chemical modification upon interaction with argon ions.

The overall stoichiometry and the distribution of Si between the different oxidation states, as obtained from the photoelectron spectra, along with the values of the modified Auger parameters of the H-rich deposits produced by cw $CO_2$ laser radiation, are given in in Table 2. It is seen that these films also are composed of of $Si^0$, $Si^x$ and $Si^{4+}$ contributions and that the film obtained with lower incident radiation energy (Run 8) contains less of the $Si^o$ form, but more $Si^{4+}$ These films thus reveal their high aptitude to undergo oxidation.

Scanning electron microscopy (SEM) analysis reveals that all the deposits, regardless of their formation under different irradiation conditions, consist of agglomerates which have a continuous structure (Fig. 9). Transmission electron microscopy (TEM) analysis confirms this fact and shows small particles *ca* 100 nm in size which are bonded together.[11] These features are consistent with the assumed polymerization of $H_2SiO$ or $H_nSiO$ species and may indicate that the polymerized agglomerates increase their size not only in the gas phase but also when they have been deposited on the substrate surface.

## Mechanism of DSO decomposition

The decomposition products silane and hydrogen, the yield of silane under the different irradiation conditions and the properties of the solid deposits

$$H_3SiOSiH_3 \rightarrow H_2Si{=}O + SiH_4$$

$$SiH_4 \rightarrow H_2 + H_2Si :\rightarrow Si/H \text{ and} (Si^0)$$

$$H_2Si{=}O \rightarrow (H_2SiO)_n$$

$$H_2Si{=}O \text{ and/or } (H_2SiO)_n \rightarrow H_2 + H/Si/O$$

**Scheme 1** IR laser-induced decomposition of DSO.[11]

$$DSO + nH_2Si{=}O \rightarrow H_3Si(OSiH_2)_nOSiH_3\ (n = 1, 2)$$

$$nH_2Si{=}O \rightarrow (H_2SiO)_n\ (n = 3, 4)$$

**Scheme 2** Possible reactions of transient $H_2Si{=}O$.

are in line with the steps of the IR laser-induced decomposition of DSO as suggested earlier[11] (Scheme 1).

Although the silanone $H_2Si{=}O$ has been proved as a gas-phase transient in ozone–silane[40] and oxygen–silane[41–43] systems, our attempts to scavenge this species as a product of its insertion reactions with dimethyl(dimethoxy)silane, 1-methyl-1-silacyclobutane, hexamethyldisiloxane and 1,1-dideuterio-1-silacyclobutane failed. The transient occurrence of silanone in our experiments is, however, strongly supported by GC–MS analysis of minor volatile products produced in the DSO

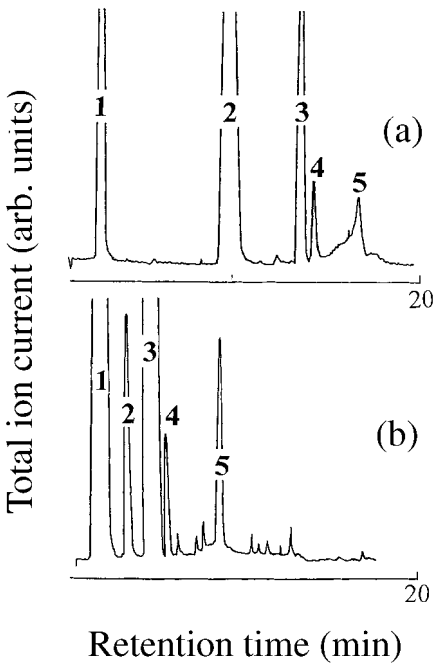


**Figure 10** Typical GC–MS trace of the mixture obtained on TEA $CO_2$ laser irradiation of (**a**) DSO (1.3 kPa)–$N_2$ (6.7 kPa); (**b**) DSO (0.7 kPa)–$(CH_3)_3SiCl$ (7.3 kPa). (**a**) Column, Porapak P; temperature programmed within 30–150 °C; peak identification: 1, $N_2$; 2, DSO; 3, $H_3SiOSiH_2OSiH_3$; 4, $(H_2SiO)_3$; 5, tentatively $H_3Si(OSiH_2)_2OSiH_3$ and $(H_2SiO)_4$. (**b**) Column, SE-30; temperature programmed within 20–150 °C; peak identification: 1, DSO; 2, $(CH_3)_3SiOSiH_3$; 3, $(CH_3)_3SiCl$; 4, $(CH_3)_3SiOH$; 5, $[(CH_3)_3Si]_2O$.

$$H_2Si{=}O \leftrightarrow H(HO)Si{:} \rightarrow P$$

$$H(HO)Si{:} \rightarrow Si^0 + H_2O$$

$$P \rightarrow \text{siloxane} + H_2O$$

$$H(HO)Si{:} + H_2 \rightarrow H_3SiOH$$

$$H_3SiOH + (CH_3)_3SiCl \rightarrow H_3SiOSi(CH_3)_3 + HCl$$

$$(CH_3)_3SiCl + H_2O \rightarrow (CH_3)_3SiOH \rightarrow [(CH_3)_3Si]_2O$$

**Scheme 3** Possible reactions of various transients involved in the decomposition of DSO. P, (products of recombination of $H_2Si{=}O$ and of insertion of H(HO)Si: into DSO.

decomposition in an excess of inert gases (helium, argon, nitrogen). The GC–MS trace (Fig. 10a) reveals very minor peaks of trisiloxane and cyclotrisiloxane, and a peak tentatively assigned to a mixture of tetrasiloxane and cyclotetrasiloxane (Table 3). These compounds can only be rationalized in terms of $H_2Si{=}O$ insertion into DSO, or of $H_2Si{=}O$ cyclotrimerization and cyclotetramerization (Scheme 2).

Additional information on transients involved in the DSO decomposition was obtained from scavenging experiments with trimethylchlorosilane, which revealed formation of trimethyldisiloxane, trimethylsilanol and hexamethyldisiloxane (Fig. 10b). These compounds are in keeping with a transient occurrence of hydroxysilylene H(HO)Si:, the species[44] earlier observed in the microwave discharge of $SiH_4$–$O_2$ mixtures,[43] arising by silanone isomerization[45–47] and yielding water with which trimethylchlorosilane reacts to yield $(CH_3)_3SiOH$ and further $[(CH_3)_2Si]_2O$. 1,1,1-Trimethyldisiloxane can only be formed by reaction of trimethylchlorosilane with silanol, $H_3SiOH$. The observation of $(CH_3)_3SiOSiH_3$ thus provides (indirectly but unequivocally) evidence for the transient existence of the simplest (yet unobserved but theoretically defined[48–51]) silanol which can only be produced[52] by reaction of hydroxysilylene with $H_2$ available in the system from dehydrogenation of silane or the $H_2SiO$ species. These steps are given in Scheme 3.

Transient occurrence of the unsaturated silicon intermediates is supported by the UV spectra of DSO irradiated with the cw $CO_2$ laser (Fig. 11a). DSO is almost transparent in the UV region, but the rise of a broad absorption band peaking at *ca* 260 nm and tailing behind 500 nm is observed

 

**Table 3** Mass fragmentation pattern[a] of minor products observed in the GC–MS traces in Fig. 13

| Compound | Mass spectrum, *m/z* (relative intensity) |
|---|---|
| $H_3SiOSiH_3$ | 78 (30), 77 (100), 76 (49), 75 (68), 74 (20), 73 (53), 72 (23) |
| $H_3SiOSiH_2OSiH_3$ | 124 (18), 123 (100), 122 (21), 121 (36), 120 (27), 119 (19), 118 (11), 91 (34), 77 (20), 75 (20), 73 (13) |
| $(H_2SiO)_3$ | 138 (18), 137 (100), 136 (46), 135 (26), 134 (17), 133 (11) |
| $(H_2SiO)_4$ and $H_3SiO(H_2SiO)_2SiH_3$[b] | 138 (24), 137 (100), 136 (82), 135 (19), 134 (11), 77 (12), 75 (10) |
| $(CH_3)_3SiOSiH_3$[c] | 105 (100), 104 (10), 103 (17), 73 (10), 59 (17) |
| $(CH_3)_3SiOH$[d] | 75 (100) |

[a] Signals of relative intensity $\geq$10%.
[b] Peak 5 in Fig. 13(a), also signals at *m/z* = 170 (2) 169 (4), 168 (2), 167 (2), 166 (2), 165 (1), 164 (1), 163 (1), 162 (1) and at *m/z* = 184 (1), 183 (1), 182 (2), 181–179 (<1).
[c] Also signals at *m/z* = 120 (1), 119 (5), 118 (1) and 117 (1); [53].
[d] Compared with an authentic sample.

when DSO is exposed to cw radiation. The band diminishes in intensity (and changes the shape) as DSO is being depleted, and finally disappears. We exclude interference between the observed spectrum with that of the concurrently deposited solid H/Si/O particles, since the UV spectrum of these solids has a narrower band at a maximum of 240 nm (Fig. 11b) and constitutes less than 10% (curve 5 in Fig. 13a) of the observed total absorption. Although the relatively long scanning interval (80 ms) may not allow assignment of the absorption band exclusively to a single species, we assume that the absorption maximum is, in analogy with ketones, mostly due to an n–$\pi$ transition of silanone.

The TEA $CO_2$ laser irradiation of mixtures of DSO–$d_6$–$SF_6$–$H_2$ and of DSO–$d_6$–$SF_6$–DSO was carried out in order to find out whether the monomolecular mechanism of the DSO decomposition determined under the conditions of the cw $CO_2$ laser irradiation[11] applies also to the conditions of the pulsed TEA $CO_2$ laser irradiation. Observation of only $SiD_4$ in the former, and of only $SiH_4$ and $SiD_4$ in the latter, would provide the evidence. FTIR spectra of the TEA $CO_2$ laser-irradiated mixtures and their comparison with those of individual $H_nSiD_{4-n}$ ($n$ = 1–4) compounds revealed that both irradiated systems yield a blend of all the silane isotopomers. This indicates that the H/D scrambling is a facile reaction, but may not exclude the possibility of H/D scrambling among the final (energy-rich) $SiH_4$ and $SiD_4$ products.

## CONCLUSION

The TEA $CO_2$ laser-induced decomposition of DSO is controlled by elimination of silane and it is postulated to yield unstable silanone which undergoes polymerization to yield poly(perhydri-

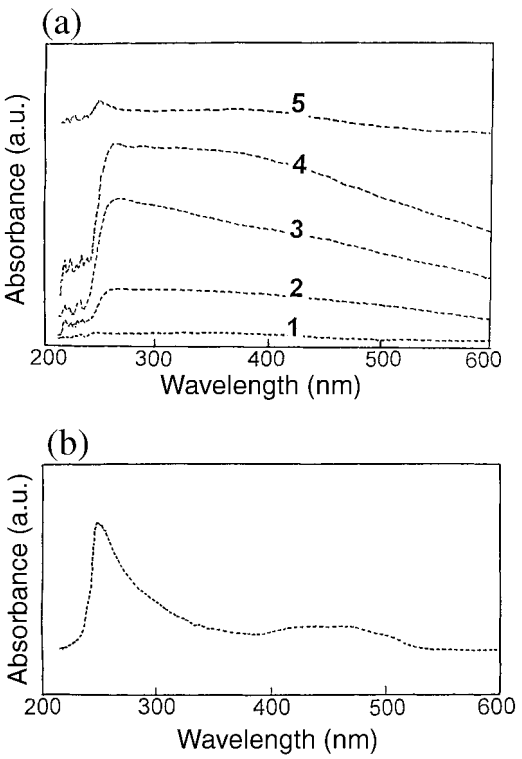


**Figure 11** (a) UV spectrum of DSO (3 kPa, irradiated with the cw $CO_2$ laser) scanned within 80 ms. Curve **1**, before irradiation; curves **2, 3** and **4** correspond, in the given order, to spectra scanned in sequence after the laser was turned on; curve **5**, after irradiation. (b) UV spectrum of the deposit obtained by irradiation of DSO with the cw $CO_2$ laser.

dosiloxane) solid films. Trapping experiments and formation of minor volatile products support the view on the involvement of $H_2Si{=}O$, (HO)HSi: and $H_3SiOH$ transients. The resulting perhydridosilicone films are produced via a multitude of reactions of the postulated $H_2Si{=}O$, (HO)HSi:, $H_2Si$: and $Si^0$ species. FTIR and XP spectra of the solid films produced under milder irradiation conditions are mostly composed of $H_2SiO$ units, whereas those deposited with high fluences are represented by an $(H_nSiO)_x$ ($n < 2$) structure and correspond to crosslinked poly(perhydridosiloxanes) with less hydrogen. The films incorporate $Si^{n+}$, ($0 < n < 4$) $Si^0$ and $Si^{4+}$ constituents. The latter observation and the ratio $Si/O > 1$ for the topmost layers are in keeping with facile oxidation of the films when exposed to the ambient atmosphere. The films can be modified by argon ion sputtering which induces formation of a new silicon suboxide state.

The TEA and cw $CO_2$ laser-induced decompositions of DSO recommend themselves as promising techniques for chemical vapour deposition of hydrogenated silicon suboxide materials with high H content, which can find important applications in electronics.

*Acknowledgements* The authors thank Professor H. Bürger for his comments on the manuscript and the availability of the spectra of silane isotopomers, and the Grant Agency of the Academy of Sciences of the Czech Republic (grant no. A4072806), the Deutsche Forschungsgemeinschaft and the Fonds der Chemischen Industrie for support.

## REFERENCES

1. Stock A, Somieski C, Wintgen R. *Ber. Deut. Chem. Ges.* 1917; **50**: 1764.
2. Stock A, Somieski C. *Ber. Dtsch. Chem. Ges.* 1919; **52**: 1851.
3. Stock A, Somieski C. *Ber. Dtsch. Chem. Ges.* 1920; **53**: 759, 766.
4. Yoshika T, MacDiarmid MG. *Inorg. Nucl. Chem. Lett.* 1969; **5**: 69.
5. Kameratos E, Lampe FW. *J. Phys. Chem.* 1970; **74**: 2267.
6. Lampe FW. *Spectrochim. Acta, Part A*, 1987; **43**: 257.
7. Lucovsky G, Yang J, Chao SS, Tyler JE, Czubatyj W. *Phys. Rev. B* 1983; **28**: 3225.
8. Tsu DV, Lucovsky G, Davidson BN. *Phys. Rev. B* 1989; **40**: 1795.
9. John P, Odeh IM, Thomas MJK, Tricker MJ, Wilson JIB. *Phys. Status Solidi B* 1981; **105**: 499.
10. Pola J, Urbanová M, Bastl Z, Šubrt J, Beckers H. *J. Mater. Chem.* 1999; **9**: 2429.
11. Pola J, Urbanová M, Drinek V, Šubrt J, Beckers H. *Appl. Organomet. Chem.* 1999; **13**: 655.
12. Hughes AE, Sexton BA. *J. Electron Spectrosc. Relat. Phenom.* 1988; **46**: 31.
13. Band IM, Kharitonov Yu I, Trzhaskovskaya MB. *Atomic Data and Nuclear Data Tables* 1979; **23**: 443.
14. Seah MP. In *Practical Surface Analysis*, Vol. 1, Briggs D, Seah MP (eds). Wiley: Chichester 1990; 201.
15. Seah MP, Dench WA. *Surf. Interface Anal.* 1979; **1**: 1.
16. Lord RC, Robinson DW, Schumb WC. *J. Am. Chem. Soc.* 1956; **78**: 1327.
17. Durig JR, Flanagan MJ, Kalasinsky VF. *J. Chem. Phys.* 1977; **66**: 2775.
18. Shaub WM, Bauer SH, *Int. J. Chem. Kinet.* 1975; **7**: 509.
19. Russell DK. *Chem. Soc. Rev.* 1990; **19**: 407.
20. Pola J, Farkacová M, Kubát P, Trnka A. *J. Chem. Soc., Faraday Trans. I* 1984; **80**: 1499.
21. Longway PA, Lampe FW. *J. Am. Chem. Soc.* 1981; **103**: 6813.
22. Jasinski M, Estes RD. *Chem. Phys. Lett.* 1985; **117**: 495.
23. Ring MA, O'Neal HE. *J. Phys. Chem.* 1992; **96**: 10848.
24. Becerra R, Walsh R. *J. Phys. Chem.* 1992; **96**: 10856.
25. Tsu DV, Lucovsky G, Davidson BN. *Phys. Rev. B* 1989; **40**: 1795.
26. Galeener FL, Lucovsky G. *Phys. Rev. Lett.* 1976; **37**: 1414.
27. Lucovsky G, Wong CK, Pollard WB. *J. Non-Cryst. Solids* 1983; **59/60**: 839.
28. Lucovsky G, Nemanich RJ, Knights JC. *Phys. Rev. B* 1978; **18**: 4228.
29. Pollard WB, Lucovsky G. *Phys. Rev. B* 1982; **26**: 3172.
30. Miller RGJ, Willis HA (eds). *Infrared Structural Correlation Tables and Data Cards*, Heyden. London, 1969.
31. Shanks H, Fang CJ, Ley L, Cardona M, Demond FJ, Kalitzer S. *Phys. Status Solidi B* 1980; **100**: 43.
32. Fischer C, Kriegsmann H. *Z. Anorg. Allg. Chem.* 1969; **367**: 219.
33. O'Keefe JF, Lampe FW. *Appl. Phys. Lett.* 1983; **42**: 217.
34. Borsella E, Fantoni R. *Chem. Phys. Lett.* 1988; **150**: 542.
35. Drínek V, Bastl Z, Šubrt J, Pola J. *Appl. Surf. Sci.* 1997; **108**: 283.
36. Alfosetti R, Lozzi L, Passacantando M, Picozzi P, Santucci S. *Appl. Surf. Sci.* 1993; **70/71**: 222.
37. Santucci S, Cordeschi E, Lozzi L, Passacantando M, Piozzi P. *J. Mater. Sci.* 1997; **12**: 100.
38. Zalm PC. *Surf. Interface Anal.* 1988; **11**: 1.
39. Hashimoto S, Hirokawa K, Fukuda Y, Suzuki K, Suzuki T, Usuki N, Gennai N, Yoshida S, Koda M, Sezaki H, Horie H, Tanaka A, Ohtsubo T. *Surf. Interface Anal.* 1992; **18**: 799.
40. Glinski R, Gole JL, Dixon DA. *J. Am. Chem. Soc.* 1985; **107**: 5891.
41. Bogey M, Delcroix B, Walters A, Guillemin J-C. *J. Mol. Spectrosc.* 1996; **175**: 421.
42. Bailleux S, Bogey M, Demuynck C, Destombes J-L, Walters A. *J. Chem. Phys.* 1994; **101**: 2729.
43. Withnall R, Andrews L. *J. Phys. Chem.* 1985; **89**: 3261.
44. Tachibana A, Fueno H, Koizumi M, Yamabe T, Fukui K. *J. Phys. Chem.* 1988; **92**: 935.

 

45. Darling CL, Schlegel HB. *J. Phys. Chem.* 1993; **97**: 8207.
46. Ma B, Allinger N, Schaefer HF. *J. Chem. Phys.* 1996; **105**: 5731.
47. Ma B, Schaefer HF. *J. Chem. Phys.* 1994; **101**: 2734.
48. Mortier WJ, Sauer J, Lercher JA, Noller H. *J. Phys. Chem.* 1984; **88**: 905.
49. Nicholas JB, Feyereisen M. *J. Chem. Phys.* 1995; **103**: 8031.
50. Sauer J, Ahlrichs R. *J. Chem. Phys.* 1990; **93**: 2575.
51. Nicholas JB, Winans RE, Harrison RJ, Iton LE, Curtiss LA, Hopfinger AJ. *J. Phys. Chem.* 1992; **96**: 10247.
52. Zachariah MR, Tsang W. *J. Phys. Chem.* 1995; **99**: 5308.
53. van Dyke CH, MacDiarmid AG. *Inorg. Chem.* 1964; **3**: 747.

 